JOURNAL OF Materials CHEMISTRY

The synthesis of mesostructured silica films and monoliths functionalised by noble metal nanoparticles

Ömer Dag,[a] Olga Samarskaya,[a] Neil Coombs[b] and Geoffrey A. Ozin[b]

[a]*Bilkent University, Department of Chemistry, 06533 Ankara, Turkey. E-mail: dag@fen.bilkent.edu.tr*
[b]*Materials Chemistry Research Group, Chemistry Department, University of Toronto, 80 St. George Street, Toronto, Ontario, Canada M5S 3H6. E-mail: gozin@chem.utoronto.ca*

Received 18th September 2002, Accepted 22nd November 2002
First published as an Advance Article on the web 12th December 2002

A lyotropic $AgNO_3$, $HAuCl_4$ and H_2PtCl_6–silica liquid crystalline (LC) phase is used as a supramolecular template for a one-pot synthesis of novel noble metal or complex ion containing nanocomposite materials in the form of a film and monolith. In these structures, Ag^+, $AuCl_4^-$ and $PtCl_6^{2-}$ ions interact with the head group of an oligo(ethylene oxide) type non-ionic surfactant ($C_{12}H_{25}(CH_2CH_2O)_{10}OH$, denoted as $C_{12}EO_{10}$) assembly that are embedded within the channels of hexagonal mesostructured silica materials. A chemical and/or thermal reduction of the metal or complex ions produces nanoparticles of these metals in the mesoporous channels and the void spaces of the silica. The LC mesophase of $H_2O:X:HNO_3:C_{12}EO_{10}$, (where X is $AgNO_3$, $HAuCl_4$ and H_2PtCl_6), and nanocomposite silica materials of *meso*-SiO_2–$C_{12}EO_{10}$–X and *meso*-SiO_2–$C_{12}EO_{10}$–M (M is the Ag, Au and Pt nanoparticles) have been investigated using polarised optical microscopy (POM), powder X-ray diffraction (PXRD), transmission electron microscopy (TEM), nuclear magnetic resonance (NMR), Fourier transform infrared (FTIR), Fourier transform (FT) Raman and UV-Vis absorption spectroscopy. Collectively the results indicate that the LC phase of a 50 w/w% $H_2O:C_{12}EO_{10}$ is stable upon mixing with $AgNO_3$, $HAuCl_4$ and H_2PtCl_6 salts and/or acids. The metal ions or complex ions are distributed inside the channels of the mesoporous silica materials at low concentrations and may be converted into metal nanoparticles within the channels by a chemical and/or thermal reduction process. The metal nanoparticles have a broad size distribution where the platinum and silver particles are very small (typically 2–6 nm) and the gold particles are much larger (typically 5–30 nm).

Introduction

Since the first report by Kresge *et al.*[1] in 1992 on mesoporous silica MCM-41 type materials the field has attracted a great deal of attention regarding mesoporous materials with new compositions[2–5] and pore modifications.[6–21] Incorporation of noble metals into the pores of MCM type materials was first attempted by Ryoo and Ko[9] in order to image the structure of MCM-41 using TEM. Later, various applications of these metal nanoparticles such as non-linear optics and catalysis promoted further studies of these mesostructured metal–silica nanocomposite materials. Recently, Ryoo *et al.* employed an impregnation method to produce high loadings of Pt within calcined MCM-48, which upon etching the silica resulted in a nanoscale Pt replica of the host material.[10] Chao *et al.* also demonstrated densely packed metal nanostructures inside $(CH_3O)_3Si(CH_2)_3N(CH_3)_3Cl$ modified MCM-41 and MCM-48. A strong electrostatic interaction between the surface $O_3Si(CH_2)_3N(CH_3)_3^+$ cationic sites and MCl_m^{n-} anions (where M is Pt or Au) promoted ion exchange between Cl^- of the surface $O_3Si(CH_2)_3N(CH_3)_3Cl$ groups and MCl_m^{n-} ions in the solution.[22]

The LC templating with the non-ionic surfactant C_nH_{2n+1}-$(CH_2CH_2O)_mOH$, (C_nEO_m) was first used in a one-pot synthesis to incorporate Li^+ and Ag^+ ions[23,24] into mesoporous silica materials. This surfactant has the advantage of dissolving metal salts and maintaining the integrity of the liquid crystalline (LC) phase during the synthesis of the mesoporous silica. A limitation of this approach is the achievable salt concentration.[23–25] Recently Dag *et al.*[25,26] demonstrated that the non-ionic surfactants (C_nEO_m) can dissolve transition metal aqua complex salts ($[M(H_2O)_x]X_y$, where M is a transition metal and X is a counter anion) without any extra water to produce hexagonal and/or cubic LC phases. The hydrogen-bonding interaction between the $[M(H_2O)_x^{2+}]$ cation and ethoxy (EO) groups of the surfactant molecules plays a key role in the formation of the LC phase.[25] In the work described herein, $AgNO_3$, $HAuCl_4$ and H_2PtCl_6 salt or acids are used in the LC phase of 50 w/w% water–surfactant. These compounds are solvated by water in the vicinity of the EO head groups of the surfactant molecules. Silica polymerisation starts in the water–surfactant–HNO_3–$Si(OCH_3)_4$ mixture and continues in the hydrophilic region of the hexagonal LC phase. This procedure yields mesoporous silica materials with Ag^+, $AuCl_4^-$ or $PtCl_6^{2-}$ ions homogeneously distributed inside the pores. The imbibed metal or complex ions were chemically and/or thermally converted to metal nanoparticles inside the pores of mesoporous silica films and monoliths.[7,27–29] Mesoporous silica materials obtained before and after reduction of the imbibed metal ions were characterised using PXRD, TEM, POM, FT-IR, FT-Raman and UV-Vis transmittance and diffuse reflectance spectroscopy techniques.

Experimental

Synthesis of mesoporous silica in the presence of Ag^+, $AuCl_4^-$ and $PtCl_6^{2-}$ ions

Silver nitrate ($AgNO_3$, 0.00–0.25 g) was dissolved in 0.70 g of water and 0.20 g of nitric acid. 1.00 g of poly(ethylene oxide) non-ionic surfactant, $C_{12}EO_{10}$, was added to the salt solution. The homogeneous transparent dense blends were obtained while heating at 40–50 °C in the oven for 20 min followed by cooling to an ambient temperature. 1.47 g of tetramethylorthosilicate

 DOI: 10.1039/b209153b

(TMOS) was prehydrolyzed in an acidic solution of 0.22 g of water and 0.02 g of nitric acid and cooled to room temperature. These two solutions were blended to obtain a homogenous mixture containing silver nitrate.

The clear, isotropic liquid solution was poured onto a glass slide and left to dry in open air, under ambient conditions. A characteristic fan-like birefringence texture was observed under POM over a silicification period of 10–60 min. Samples were kept in the dark for three days before investigation. The fan-like optical texture was preserved during the curing of the silica network. In this work three different substrates were used: silicon, Si(100) wafers to make thin films for FT-IR measurements; glass slides for recording POM images; and quartz windows for UV-Vis spectroscopy.

The same procedure was applied to $HAuCl_4$ and H_2PtCl_6. Like $AgNO_3$, the $HAuCl_4$ and H_2PtCl_6 systems also form an LC phase at low metal ion/surfactant ratios under the above reaction conditions. Since $HAuCl_4$ is not very stable under ambient laboratory conditions, polymerisation of the silica was carried out in the dark. The mesostructured thin films obtained from these systems are transparent and colourless for $AgNO_3$, yellow for $HAuCl_4$ and orange for H_2PtCl_6.

Reduction of Ag^+, $PtCl_6^{2-}$ and $AuCl_4^-$ in mesoporous silica

In order to reduce Ag^+ ions in the channels of mesoporous silica thin films, the samples deposited onto quartz windows and silicon wafers were exposed to hydrazine (N_2H_4) vapour. The appearance and growth of silver particles was studied by using UV-Vis and FT-IR spectroscopy and POM. The optical properties of silver nanoparticles were investigated by following the evolution of the surface plasmon resonance (SPR) absorption band over a period of time until the SPR peak remains unchanged. Similarly $AuCl_4^-$ and $PtCl_6^{2-}$ ions were reduced either using hydrazine or H_2 around 100 °C.

Characterisation

The POM images were recorded in transmission mode on Meije Techno ML9400 and Stereo Stemi 2000 microscopes using convergent white light between parallel and crossed polarisers. The PXRD patterns were obtained on a Siemens D5000 diffractometer using a high power Cu-K_α source operating at 50 kV/35 mA and/or Rigaku Miniflex diffractometer using high power Cu-K_α source operating at 30 kV/15 mA. The TEM images were obtained using a Philips 430 microscope operating at an accelerating voltage of 100 kV. The samples were embedded in epoxy resin and microtomed. The FT-Raman spectra were recorded from samples in capillary glass tubes using a Bomems MB-157 FT-Raman spectrometer with an InGaAs near-IR detector. The light source was a Spectra Physics diode pumped Nd : YLF laser emitting at 1064 nm with a 350 kHz repetition rate. Notch filters covering 150–3750 cm^{-1} were used to block the Rayleigh scattering. The instrument was configured in 180° back scattering mode. The micro-Raman spectra were obtained on an S. A. LabRam confocal Raman microscope. The signal collected was transmitted through a fibre optic cable into a single grating spectrometer equipped with a 1024 × 256 element CCD. The Raman spectra were collected by manually placing the probe tip near the desired point of the film. The FT-IR spectra were recorded using a Bomem Hartman MB-102 model FTIR spectrometer. The UV-Vis absorption spectra were recorded both in diffuse reflectance and transmittance modes using Perkin-Elmer Lambda 900 and Varian Cary 5 double beam spectrometers, respectively.

Results and discussion

The formation and preservation of the LC phase as a template in the silica polymerisation is the first and crucial step in tailoring the mesoporous silica materials. In order to determine the optimum conditions for the synthesis of silver, gold and platinum functionalised mesoporous silica, this work is divided into two parts. In the first part, the properties of the $AgNO_3$–$C_{12}EO_{10}$: H_2O (50 w/w%) : HNO_3,[24] $HAuCl_4$–$C_{12}EO_{10}$: H_2O (50 w/w%) : HNO_3, and H_2PtCl_6–$C_{12}EO_{10}$: H_2O (50 w/w%) : HNO_3 mesophases were studied. The second part is devoted to tailoring the silica framework using knowledge of the system developed in the first step. In a $C_{12}EO_{10}$–H_2O system, the sequence of the mesophases follows the hexagonal (H_1)→cubic (V)→lamellar (L) order with increasing surfactant concentration at room temperature. The hexagonal LC phase is stable and appears in a wide range of surfactant concentrations (40–70 w/w%). However, the work described herein is limited to the hexagonal phase with a $C_{12}EO_{10}$: H_2O ratio of 50 w/w%.

The hexagonal LC phase of the $C_{12}EO_{10}$: H_2O (50 w/w%) binary system was determined using POM and XRD techniques. The primary identification of the LC phase involves a magnified view of a thin sample of mesogenic material placed between crossed polarisers. The arrangement of surfactant molecules was identified by the microscopic texture. The hexagonal LC phase displays a fan optical birefringence texture between the crossed polarisers (Fig. 1(A)). One can observe an alternation of bright and dark regions.

Phase properties of $C_{12}E_{10}$ surfactant in the presence of $AgNO_3$, $HAuCl_4$ and H_2PtCl_6

The lyotropic liquid crystalline phase of C_nEO_m type surfactants is a good template for the synthesis of mesoporous silica and imbibed nanoscale metal particles.[5,23,24] A key question is how much $AgNO_3$, $HAuCl_4$ and H_2PtCl_6 can be introduced into the hexagonal mesophase of $C_{12}EO_{10}$: H_2O (50 w/w%) : HNO_3 without affecting the mesostructure?[24]

The mesophases that exist in silver nitrate–$C_{12}EO_{10}$: H_2O (50 w/w%) : HNO_3 mixtures were defined by studying a range of $0.0 \leqslant r \leqslant 2.0$ samples, where r is the $AgNO_3$–$C_{12}EO_{10}$ mole ratio. To visualise mesophases heated samples were monitored

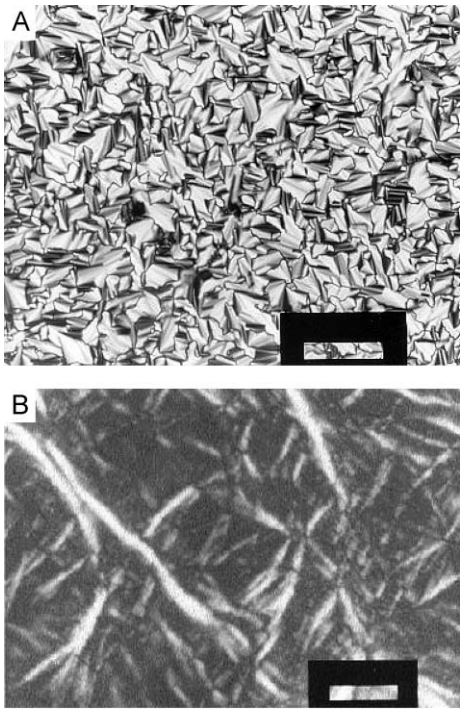

Fig. 1 POM images recorded between the crossed polarisers of $AgNO_3$: $C_{12}EO_{10}$: H_2O samples with Ag^+–$C_{12}EO_{10}$ mole ratios of (A) 0.0 to 0.8, fan texture, (B) 0.8 to 1.2 phase separated solid phase (scale bar is 200 μm).

by POM. Upon cooling the heated isotropic liquid, the optical texture of the sample emerges (Fig. 1(A)).

The mixture of $C_{12}EO_{10}$: H_2O (50 w/w%) : HNO_3 with no silver ions ($r = 0.0$ Ag^+–$C_{12}EO_{10}$ mole ratio) displays fan optical birefringent texture. The clear, transparent, dense gel with $0.0 \leqslant r \leqslant 0.6$ range (r is Ag^+–$C_{12}EO_{10}$ mole ratio) and weakly opaque gels with the $0.6 < r \leqslant 0.8$ range display optical fan texture. The liquid-like samples at higher ratios ($0.8 < r \leqslant 1.2$) are weakly anisotropic and/or do not display birefringent fan texture between crossed polarisers. POM images of solid-like high $AgNO_3$ containing samples ($1.5 \leqslant r \leqslant 2.0$) are anisotropic but do not have a fan optical texture (Fig. 1(B)).

Samples with an Ag^+–$C_{12}EO_{10}$ mole ratio of 0.7 and below became isotropic after $\sim$10 h aging under ambient conditions. Random, optically birefringent regions with different shapes and forms were observed for $0.7 \leqslant r \leqslant 0.9$ mole ratios, upon aging. However, the samples of $1.5 \leqslant r < 2.0$ preserve their initially formed anisotropic optical textures during aging (Fig. 1(B)). The samples, which were sealed in vials and kept in the dark, also undergo changes. The aged mixtures of up to 0.8 $AgNO_3$–$C_{12}EO_{10}$ mole ratios remained unaltered. However, a white solid formed at the air–LC interface, over the transparent gel phase, from $r = 0.9$ and at the bottom of the mixture, from $r = 1.2$. The gel phase of all these mixtures display fan texture and the solid phase is crystalline and anisotropic.

At higher concentrations and/or with time, the mixture undergoes phase separation producing a crystalline $Ag(C_{12}EO_{10})_xNO_3$ complex.[22] The remaining less concentrated (r is no longer as large as the starting mixture) phase is transparent and liquid crystalline with an optical fan texture in POM. This is simply due to the solubility of $AgNO_3$ in a water–surfactant system and coordination of the Ag^+ ion with the surfactant ethoxy groups. Initially formed supersaturated mixture yields precipitation of the complex over time.[22]

The metal–oxygen interaction imparts a slight cationic character to the head groups.[30–32] Thus we could trace the effect of added salt to the $C_{12}EO_{10}$: H_2O (50 w/w%) : HNO_3 system by investigating the ethylene oxide $(EO)_m$ units. FT-IR spectroscopy informatively reveals the presence of hydrogen bonds, conformation changes of the ethoxy head groups and the phase changes. It was found that the strength of hydrogen bonding between water and the EO chain of the surfactant molecules follows the order, liquid < mesophase < solid.[33] Detailed studies of carbon–hydrogen stretching (ν-CH_2) modes and carbon–hydrogen bending (δ-CH_2) modes in the regions between 2820 and 2960 cm^{-1}, and 1220 and 1500 cm^{-1}, respectively, provide information about local environment of the poly(ethylene oxide) head group. Spectral changes upon evaporation of the water molecules are drastic with the aging of $AgNO_3$: H_2O : $C_{12}EO_{10}$ mixtures (Fig. 2). The change in the IR spectra of the samples with low $AgNO_3$ concentrations ($0.1 = r < 0.4$ of $AgNO_3$–$C_{12}EO_{10}$ mole ratios) is not very significant but some of the peaks become sharper and better resolved as the solvent is evaporated (Fig. 2). Significant changes are traced in the IR spectra of mixtures ($r \geqslant 0.5$) before and after water evaporation (Figs. 2 and 3).

Addition of $AgNO_3$ to the LC phase of the $C_{12}EO_{10}$: H_2O (50 w/w%) : HNO_3 mixture causes a broadening of the bands in the δ-CH_2 deformation region of the $C_{12}EO_{10}$. In the LC phase of the $AgNO_3$: $C_{12}EO_{10}$: H_2O (50 w/w%) : HNO_3, this region contains surfactant related peaks and a broad peak at around 1380 cm^{-1} due to asymmetric stretching mode of free nitrate ions. However, with the evaporation of water molecules and increasing of silver nitrate in the $AgNO_3$: $C_{12}EO_{10}$: H_2O (50 w/w%) : HNO_3 mixture, one can observe the development of sharp and intense IR bands. With aging, the peaks at 1467, 1446, 1350, 1305 and 1250 cm^{-1} dominate in the δ-CH_2 spectral region of the samples in the gel phase (Figs. 2 and 3).

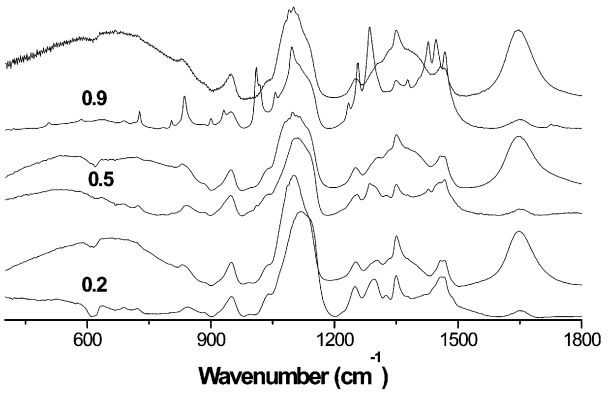

Fig. 2 FT-IR absorption spectra of the freshly prepared liquid crystalline $AgNO_3$–$C_{12}E_{10}$: H_2O (50 w/w%) : HNO_3-top spectra, aged mixture of the $AgNO_3$–$C_{12}E_{10}$: H_2O : HNO_3-bottom spectra in each group. The Ag^+–$C_{12}E_{10}$ molar ratios indicated along the spectra.

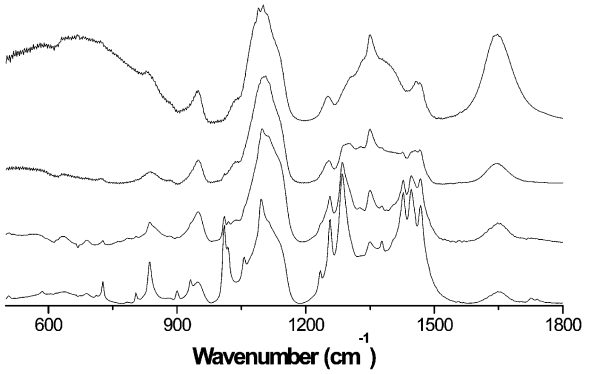

Fig. 3 FT-IR spectra recorded from the LC phase of $AgNO_3$: $C_{12}E_{10}$: H_2O : HNO_3 ($r = 0.9$) upon water evaporation and aging from top to bottom.

The peaks at 1467, 1446, 1427, 1286, 1256 and 1234 cm^{-1} are related to the solid phase that co-exists with the LC phase in the samples.

Sharpening of the peaks is due to complex formation, aggregation and crystallisation of the material in the form of $Ag(C_{12}EO_{10})_xNO_3$ complex.[22] On the basis of the IR data and literature assignments[33–36] it is clear that upon increasing the silver nitrate concentration, there is a phase transition of the $AgNO_3$–$C_{12}EO_{10}$: H_2O (50 w/w%) : HNO_3 system from the hexagonal LC phase, which appears as a clear dense gel, to another phase, which is a white soft solid. It is apparent that the Ag^+ and NO_3^- ions both play very important roles in the collapsing of H_1 LC phase through altering the hydrophilicity of the EO head group. If this is true, one would expect a red-shift in the C–O–C stretching mode, observed at 1116 cm^{-1} from the amorphous pure polyether phase.[33] A broad peak, centred at 1096 cm^{-1} (Fig. 3) confirms the interactions between EO groups and Ag^+ ions, leading to the formation of transient cross-links, which weaken the C–O polyether bonds. The peaks at 1130, 1096, 1078 cm^{-1} in the ν–C–O stretching vibration region, suggest that the silver ions interact with the EO head groups with different strengths, thereby stiffening the EO chain and inducing a phase transition. The sharp and intense peaks, which are due to various interactions of the EO group and Ag^+ ions, appear at around 700–1000 cm^{-1}. This is also evident from the nitrate symmetric stretching mode observed at around 1010–1030 cm^{-1}. The peaks observed in this region show that the nitrate ion is interacting with the Ag^+ ion both as a bidentate and/or unidentate ligand. It is the coordination that causes the $AgNO_3$ system in the LC phase to undergo phase separation and crystallisation into white solid matter.

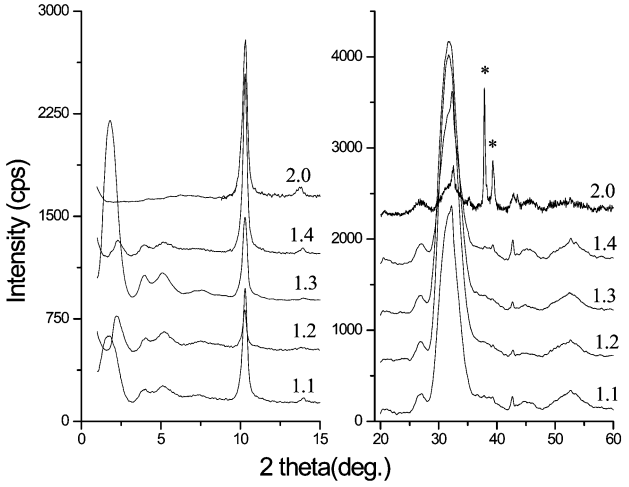

Fig. 4 PXRD of the complex $Ag(C_{12}EO_{10})_xNO_3$ in the low and high angle region (the numbers indicate the $AgNO_3$–$C_{12}EO_{10}$ mole ratio in the samples).

It was discovered that the silver and nitrate ions affect the phase properties of the $C_{12}EO_{10}$: H_2O (50 w/w%) : HNO_3 system through the formation of a $Ag(C_{12}EO_{10})_xNO_3$ complex.[22] The splitting of the nitrate asymmetric and bending modes at around 1200–1500 cm^{-1} and 710–730 cm^{-1}, respectively, and the combination band of the nitrate symmetric stretching and the bending modes observed at around 1720–1750 cm^{-1} (Fig. 3) also provide strong evidence for the above proposal.[37]

PXRD patterns were also recorded for samples with various $AgNO_3$–$C_{12}EO_{10}$ mole ratios. The PXRD patterns display broad lines at both low and high angles (Fig. 4). Note that the LC phase does not diffract at high angles. It is clear from the PXRD that the solid white precipitate is crystalline which is consistent with the IR interpretations.

Similarly the $HAuCl_4$: $C_{12}EO_{10}$: H_2O and H_2PtCl_6 : $C_{12}EO_{10}$: H_2O systems were studied using POM, FT-Raman and UV-Vis absorption spectroscopy. The POM images display fan-texture for both mixtures between the cross-polarisers. However, the behaviour of these two systems is different than that of the silver one. There is no complex formation or phase separation observed in these two systems. In the case of $HAuCl_4$, the samples are not stable under ambient conditions, over time hexagonal and/or triangular gold plates form with sizes greater than a micron. At higher $HAuCl_4$ concentrations the LC phase does not survive. Around 0.5–0.6 $AuCl_4^-$: surfactant mole ratio the LC phase is stable and can be used as a template for the silica polymerisation. This ratio is not very different to the case of H_2PtCl_6.

The procedure described above allows one pot synthesis of film/monoliths of mesoporous silica modified with Ag^+, $AuCl_4^-$ and $PtCl_6^{2-}$ ions by controlling the amount of metal or complex ions in a certain concentration range. The mesophase of H_2PtCl_6 in $C_{12}EO_{10}$: H_2O (50 w/w%) is quite stable at higher mole ratios and the phase transition temperature increases with increasing H_2PtCl_6 concentration.[38] Upon addition of the silica source, the more concentrated mixtures yield disordered silica materials. Again the 0.5–0.6 H_2PtCl_6–$C_{12}EO_{10}$ mole ratio, is the largest concentration for forming ordered mesoporous silica materials.

Mesoporous silica templated by $AgNO_3$: $C_{12}EO_{10}$: H_2O, $HAuCl_4$: $C_{12}EO_{10}$: H_2O and H_2PtCl_6 : $C_{12}EO_{10}$: H_2O LC phases.

The addition of the silica source, TMOS to any one of the $AgNO_3$: $C_{12}EO_{10}$: H_2O : HNO_3, $HAuCl_4$: $C_{12}EO_{10}$: H_2O : HNO_3 and H_2PtCl_6 : $C_{12}EO_{10}$: H_2O : HNO_3 mixtures first creates a clear solution. However in 10–20 min, upon casting them on a glass slide, silicon wafer or a quartz window, the mixtures form a hexagonal LC phase. The pre-hydrolyzed silica species most likely terminated by SiOH surface sites together with the evaporation of CH_3OH (hydrolysis product of TMOS) reorganise the system back to the LC phase. Further polymerisation of these silica species continues in the LC hydrophilic regions of the mesophase to yield mesostructured silica materials.[5] A typical ^{29}Si MAS NMR spectrum of a sample, obtained through the above procedure, shows that the film or monolithic mesoporous silica is not fully polymerised.[23] The bands, observed at 92, 101 and 110 ppm with respect to tetramethylsilane (TMS) with 9.5, 50.3 and 40.2% of the total ^{29}Si signals corresponding to Q_2 $O_2Si(OH)_2$, Q_3 O_3SiOH and Q_4 SiO_4 sites, respectively, confirm that the silica polymerisation is not complete.

Similarity between the optical textures of the materials before and after the addition of the silica source and upon formation of mesostructured silica, predetermines the hexagonal arrays of pores in the solid materials.[22,23] The changes in the POM images, taken over time, suggest continuous polymerisation/condensation of silicate even a month after the film deposition.

The FT-IR absorption spectra recorded for freshly prepared thin films of the $AgNO_3$–$C_{12}EO_{10}$: H_2O (50 w/w%) : HNO_3–TMOS mixture of $0.0 < r \leqslant 0.9$ Ag^+–$C_{12}EO_{10}$ mole ratios have been discussed extensively.[22] Appearance of sharp well-resolved features at 1467, 1446, 1427, 1286, and 1256 cm^{-1} detected by FT-IR for the sample with higher silver content ($r = 0.9$ Ag^+–$C_{12}EO_{10}$ mole ratio) is a good indication for the phase separation of the template mixture associated with the formation of the $Ag(C_{12}EO_{10})_xNO_3$ complex.[22] Usually crystals of the complexes are formed at the surface of the film samples and can be removed by wiping.

Inspection of the PXRD patterns of the samples with different $AgNO_3$ contents reveals the existence of sharp, intense diffraction lines at low angles. The samples prepared on glass slides and/or Si(100) surface diffract at low angles and the diffraction intensity strongly depends on the orientation of the sample with respect to the detector of the diffractometer. Fig. 5(A) shows diffraction patterns of different orientation with respect to the diffractometer detector recorded from a film sample that has 0.4 mole ratio of $AgNO_3$–$C_{12}EO_{10}$. The sum of the three different positions of the film sample resembles the powder pattern. Deconvolution of the PXRD patterns reveals three reflections corresponding to 47.5, 44.9 and 42.9 Å d-spacings and indexed to (100), (002) and (101) planes of the $P6_3/mmc$ space group of a 3D-hexagonal mesoporous silica.[39–41] The unit cell parameters obtained from the diffraction patterns are $a = 54.9$, $c = 89.6$ with a $c/a = 1.633$ consistent with the 3-D hexagonal lattice structure. In samples with high silver concentration, the number of PXRD reflections can be as high as eight. These samples strongly diffract at low angles and show distinct reflections at 1.93, 2.06 and 2.22° and weak lines at 2.65, 3.81, 3.91, 3.99 and 4.21° indexed to (100), (002) and (101) and (102), (200), (112), (004) and (202) planes, respectively, of the same space group, Fig. 5(B). The effect of the salt concentration on the unit cell parameters and to the crystallinity requires further studies.

The FT-Raman spectra of samples prepared using H_2PtCl_6 display peaks corresponding to the $PtCl_6^{2-}$ ion at 346 cm^{-1} and 322 cm^{-1}. However the $AuCl_4^-$ containing samples are decomposed in the laser beam. The UV-Vis absorption spectra recorded in diffuse reflectance mode display bands which correspond to $AuCl_4^-$ ion at around 490 (shoulder), 400 (shoulder) and 333 nm due to d-d and charge transfer transitions of the $AuCl_4^-$ ions, respectively (Fig. 6). Both FT-Raman and UV-Vis absorption spectra show that $AuCl_4^-$ and $PtCl_6^{2-}$ ions are stable before reduction in the freshly prepared mesostructured silica materials. The mesophase of the H_2PtCl_6 : $C_{12}EO_{10}$: H_2O is stable at higher H_2PtCl_6

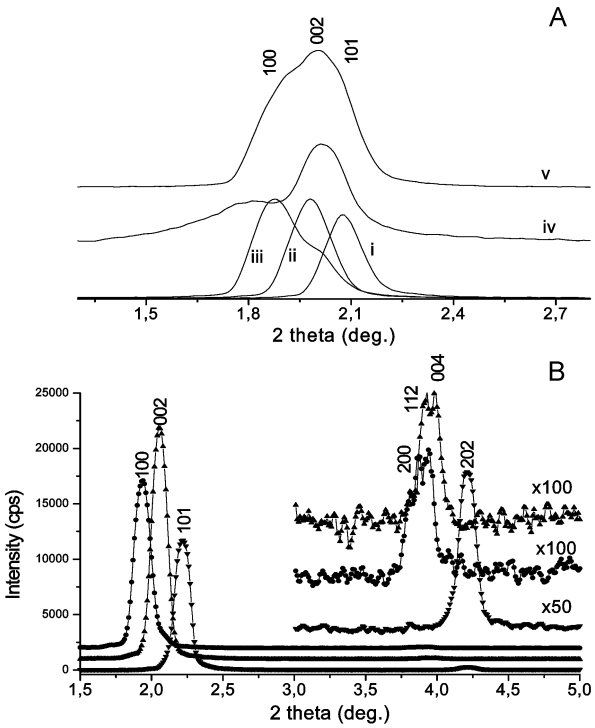

Fig. 5 (A) The PXRD pattern of oriented and crushed mesoporous silica materials of Ag–Meso–SiO_2 (unreduced) with $AgNO_3$–$C_{12}EO_{10}$ mole ratio of 0.4, (i), (ii), (iii) were run in different orientation of the film samples to the detector axis, (iv) is the crushed sample (powder) and (v) is the sum of all orientation (sum of i, ii, iii). (B) XRD patterns of oriented film sample of a 0.7 $AgNO_3 : C_{12}EO_{10}$ mole ratio (The XRD patterns were recorded by rotating the samples with respect to the detector axis).

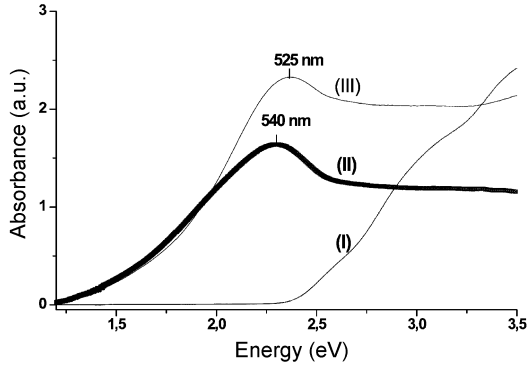

Fig. 6 UV-Vis Diffuse reflectance spectra of (I) unreduced $AuCl_4^-$ ion containing mesoporous silica, (II and III) gold samples after reduction by Si_2H_6 of two different samples, thick line (II) corresponds to 0.17 Au/surfactant ratio and thin line (III) to 0.74 mole ratio. Note also that the spectra upon reduction with N_2H_4 are very similar.

concentrations[38] but the mixture of $H_2PtCl_6 : C_{12}EO_{10} : H_2O$: TMOS never forms a LC phase at concentrations higher than 0.5–0.6 $H_2PtCl_6 : C_{12}EO_{10}$ mole ratios. Therefore the concentration of H_2PtCl_6 acid was kept low as in the case of $HAuCl_4$ and $AgNO_3$. One reason for the non-existence of the LC phase in the mixture of $H_2PtCl_6 : C_{12}EO_{10} : H_2O$: TMOS could be the acid concentration, which plays a major role in the polymerisation reaction of the silica source. Since the H_2PtCl_6 is another acid source, the rate of hydrolysis and polymerisation reaction of TMOS increases and yields dense silica before the silica species organise into mesophase. We have also investigated the incorporation of the metal and complex ions into the mesostructured titania materials using a similar one pot synthesis approach.[26]

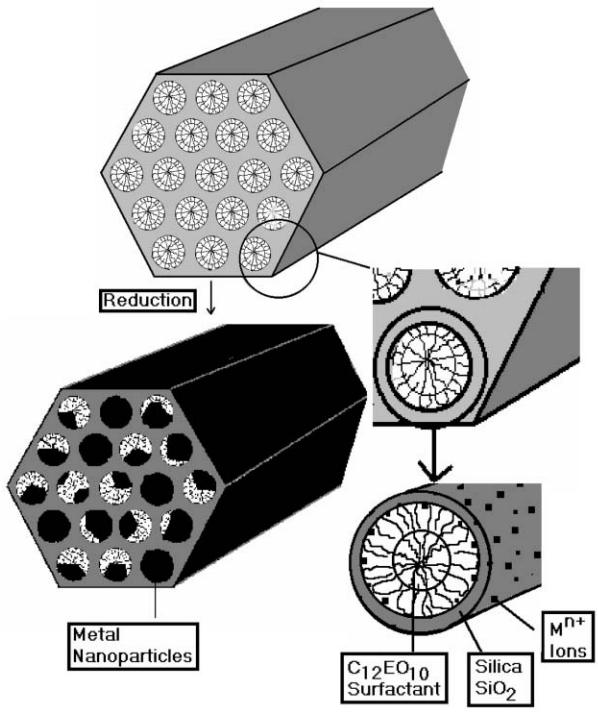

Fig. 7 Schematic representation of a hexagonal mesoporous silica material before and after reduction of metal or complex ions.

Reduction of Ag(I), Au(III) and Pt(IV) in the mesoprous silica materials (*meso*-SiO_2–$C_{12}EO_{10}$–M).

Reduction of the noble metal ions or complex ions inside the channels of mesoporous silica materials was carried out using N_2H_4 vapour in a closed container, Si_2H_6 under vacuum, $NaBH_4$ in water and in a H_2 gas flow at 100 to 150 °C. The process is schematically represented in Fig. 7. The structure of the noble metal ion or complex ions containing mesoporous silica does not alter during the reduction process under N_2H_4 (Fig. 8). All samples before and after the reduction process display similar PXRD patterns (Fig. 8). The Ag nanoparticles so formed diffract at around 38.0 and 44.2° which correspond to (111) and (200) lines of silver metal. Since wiping these samples removes the silver related diffraction lines, they likely belong to larger silver particles formed at the surface of the film samples (Fig. 8c). The samples heated at 100 °C and 450 °C still diffract at low angles, indicating that the mesostructure is stable upon calcination.

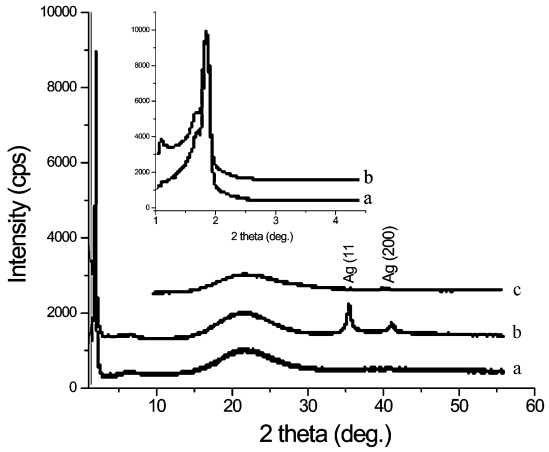

Fig. 8 PXRD pattern of 0.4 $AgNO_3$–$C_{12}EO_{10}$ templated mesoporous silica material (a) before, (b) after the reduction by hydrazine and (c) after wiping the reduced sample.

Silver ions are sensitive to their surroundings and can be thermally, photo-chemically and chemically reduced. Samples, used for reduction, were thin films deposited on glass or quartz windows. The thin film samples stored in closed containers in the dark remain colourless if the concentration of silver nitrate is low and are white at high $AgNO_3$ concentrations. We have observed that the colour of the samples exposed to air (but not to the light) changes in the following sequence: colourless pale orange brown as Ag^+–$C_{12}EO_{10}$ mole ratios increases 0.1→0.2→0.3–0.4→0.5–0.9, respectively. The colourless and white samples before exposure to the reducing agent show no plasmon band (at around 400 nm) in their UV-Vis absorption spectra, while the coloured samples display a broad plasmon band, which splits into two at ~420 nm and ~458 nm. The band at 420 nm becomes sharper as the concentration of silver nitrate increases and dominates in the spectra of the samples of $r \cong 0.7$ and up to 0.9.

UV-Vis spectroscopy was used to monitor the formation and growth process of the silver nanoparticles in the mesoporous silica matrix with time under hydrazine, N_2H_4 vapour (Fig. 9). The colour of film samples changes in the following sequence, colourless→pink→orange→yellow→brown→black with the reduction time. The UV-Vis absorption spectra of samples with Ag^+–$C_{12}EO_{10}$ mole ratios up to 0.7 reflect the evolution of the plasmon absorption band with reduction time, namely a monotonic increase in intensity and blue shifting. The white samples with high silver content $r \geqslant 0.8$ display complex spectra during the initial stages of the reduction (Fig. 9(A)). However, the evolution of the plasmon band of the coloured samples resembles those observed for samples with lower mole ratios ($r < 0.8$ silver content) (Fig. 9(B)). Despite particular differences in position, intensity, and width of the plasmon band as the concentration of silver changes from $r = 0.1$ to $r = 0.9$ with the reduction, common features are also present.

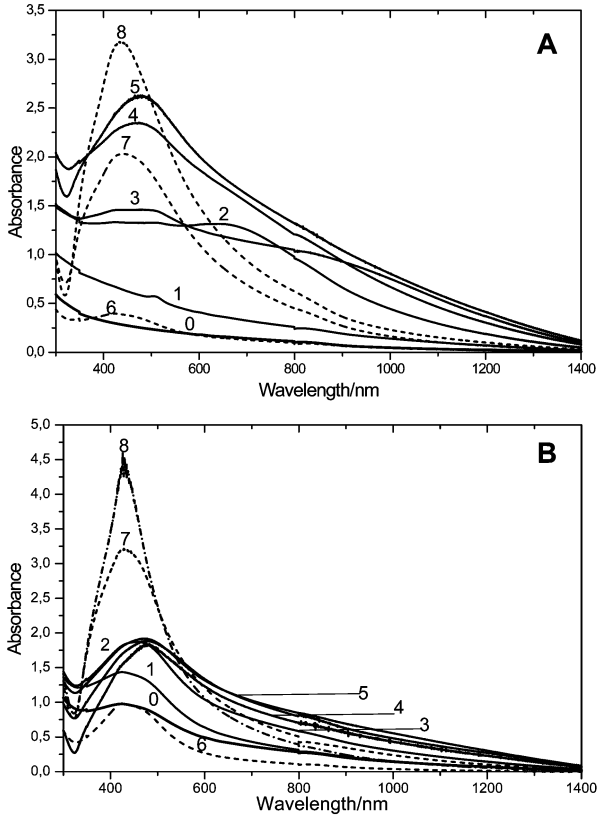

Fig. 9 UV-Vis absorption spectra for (A) white and (B) brown *meso*-SiO_2 containing 0.9 Ag^+–$C_{12}E_{10}$ molar ratio upon reduction. Dashed lines (6, 7, 8) refer to the prolonged reduction after removing of silvery mirror surface layer.

The presence of several peaks in the UV-Vis spectra of reduced white samples, especially for films with $r \geqslant 0.8$ implies different rates of reduction. Observation of two shoulders suggests that silver nanoparticles have two main environments on the outer surface and in the pores of the films. The observed shift of the plasmon band with respect to bulk silver metal provides evidence that the silver particles are in the nanometre size range and likely stabilised by either surfactant molecules and/or silica matrix (Fig. 9). The low energy feature appears from wiping experiments to originate from surface confined silver nanoparticles.

It is very well known that the colour of metal nanoparticles originates from collective effects of visible light absorption and scattering. Mie's theory explains the dependence of these effects on the particle size. However, direct correlation between metal particle size and colour of the film samples after reduction and wiping are not valid for many-particle systems, where the optical absorption is determined by both properties of individual structural units and collective effects due to interaction among the particles. Understanding the details of the processes that take place in $AgNO_3$ containing mesostructured silica materials during reduction of silver requires additional studies.

In the case of H_2PtCl_6 containing samples, the $PtCl_6^{2-}$ ions are very stable and do not undergo any reduction in air. However the $HAuCl_4$ containing samples slowly undergo reduction under ambient conditions and usually grow into micron sized gold single crystals. Keeping the $HAuCl_4$ containing silica materials in dark prevents the self-reduction. Using reducing agents and/or thermal treatments, creates small Pt nanoparticles imbibed in the pores of the silica matrix, Pt-*meso*-SiO_2. The TEM images of the Pt-*meso*-SiO_2 show 2–3 nm particles (Fig. 10(A) and (B)). However reduction under H_2 at 100 °C typically yields particles as large as the pore size of the silica matrix (Fig. 10(C)). The gold particles usually grow to much larger sizes. Careful inspection of TEM images of the gold samples, show gold particles up to 20 nm in size outside the material and smaller ones inside the pores (Fig. 10(D)).

The UV-Vis diffuse reflectance spectra of the gold nanoparticles are shown in Fig. 6. It is worth mentioning that the samples prepared with high $AuCl_4^-$ are disordered, but the less concentrated solutions produce ordered mesostructured materials. The bands observed at 525 and 540 nm are due to the plasmon mode of the gold nanoparticles in the disordered, higher gold containing samples and ordered, less concentrated samples, respectively (Fig. 6). Most likely at higher concentrations some of the $AuCl_4^-$ ions accumulate out side the pores during the silica polymerisation and produce much larger particles upon reduction on the surface of the materials. It is well known that the plasmon band blue shifts and becomes sharper when the gold particle size incerases.[42] The platinum samples usually display a broad band without a plasmon mode. All the samples of Pt containing mesoporous silica materials are black in colour and show a homogeneous distribution of very small Pt nanoparticles in the mesoporous silica materials.

Conclusion

In summary, the methods used in this work, have two advantages—first, one can produce thin films of noble metal nanoparticles embedded mesoporous silica and second, the amount of metal ions can be controlled within a certain concentration range of the metal or complex ions. We have demonstrated that noble metal nanoparticles inside the channels of the mesostructured silica materials can be prepared and the metal concentration can be controlled through the true LC templating approach.[24] The Ag and Pt nanoparticles remain small in the silica maxtrix, however, the gold particles grow to much larger sizes during the reduction process. This work shows that the incorporation of various metal ions, ionic

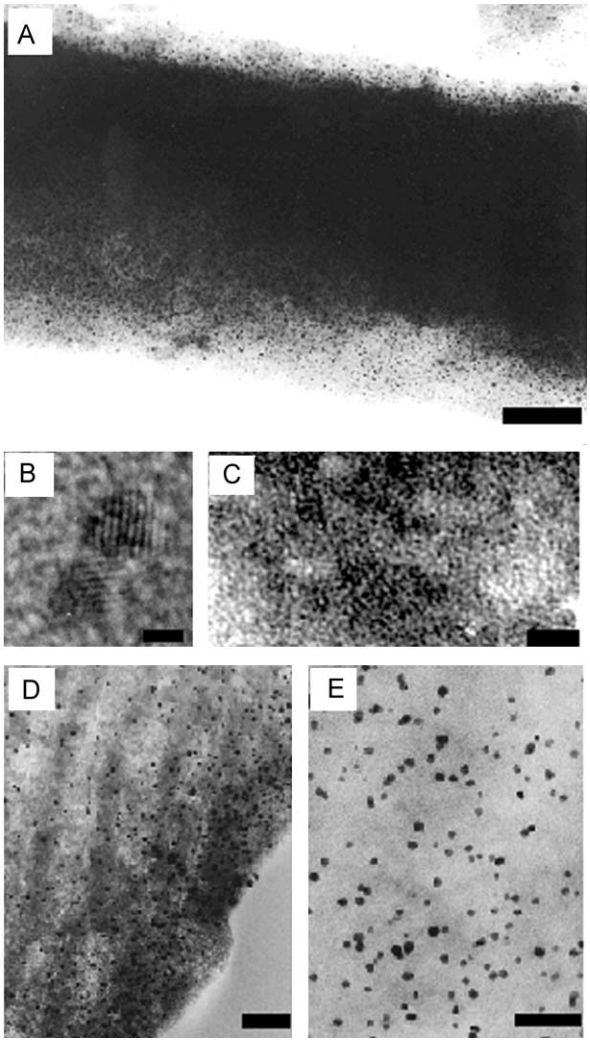

Fig. 10 TEM images of the mesoporous silca materials upon reduction. (A) Pt, scale bar is 50 nm, middle two images are different magnification of the Pt nanoparticles in the silica matrix (B) is the high resolution TEM image of the Pt particles, showing the Pt metal lattice, scale bar is 2 nm and (C) scale bar is 20 nm. The bottom images are (D) Au, scale bar is 200 nm and (E) Ag, scale bar is 50 nm.

compounds, water soluble dyes and so forth are all feasible through true LC approaches[24] for producing new functional mesoporous silica materials.

Acknowledgements

ÖD gratefully acknowledges the Scientific and Technical Research Council of Turkey (TÜBİTAK) for the financial support in the framework of Project TBAG-1812 and the Faculty Development grant of Bilkent University. GAO is Government of Canada Research Chair in Materials Chemistry. He is deeply indebted to the Natural Sciences and Engineering Council for financial support of this work.

References

1 C. T. Kresge, M. E. Leonowicz, W. J. Roth, J. C. Vartuli and J. S. Beck, *Nature*, 1992, **359**, 710.
2 Y. Lu, H. Fan, A. Stump, T. L. Ward, T. Rieker and J. Brinker, *Nature*, 1999, **398**, 223.
3 P. Yang, D. Zhao, D. I. Margolese, B. F. Chmelka and G. D. Stucky, *Nature*, 1998(396), 152.
4 H. Yang, A. Kuperman, N. Coombs, S. Mamiche-Afara and G. A. Ozin, *Nature*, 1996, **379**, 705.
5 G. S. Attard, J. C. Glyde and C. G. Göltner, *Nature*, 1995, **378**, 366.
6 E. Chomski, Ö. Dag, A. Kuperman and G. A. Ozin, *Chem. Vap. Deposition*, 1996, **2**, 8.
7 Ö. Dag, G. A. Ozin, H. Yang, C. Reber and B. Guillaume, *Adv. Mater.*, 1999, **6**, 474.
8 R. Leon, D. Margolese, G. D. Stucky and P. M. Petroff, *Phys. Rev. B: Condens. Mater*, 1995, **52**, R2285.
9 C. H. Ko and R. Ryoo, *Chem. Commun.*, 1996, 2467.
10 H. J. Shin, R. Ryoo, Z. Liu and O. Terasaki, *J. Am. Chem. Soc.*, 2001, **123**, 1246.
11 L.-Z. wang, J.-L. Shi, W. H. Zhang, M. L. Ruan, J. Yu and D. S. Yan, *Chem. Mater.*, 1999, **11**, 3015.
12 Y. J. Han, J. M. Kim and G. D. Stucky, *Chem. Mater.*, 2000, **12**, 2068.
13 A. Sayari, *Chem. Mater.*, 1996, **8**, 1840.
14 T. Hirai, H. Okubo and I. Komosawa, *J. Phys. Chem. B*, 1999, **103**, 4228.
15 S. A. Johnson, D. Khushalani, N. Coombs, T. E. Mallouk and G. A. Ozin, *J. Mater. Chem.*, 1998, **8**, 13.
16 Z. Liu, Y. Sakamoto, T. Ohsuna, K. Hiraga, O. Terasaki, C. H. Ko, H. J. Shin and R. Ryoo, *Angew. Chem. Int. Ed.*, 2000, **39**, 3107.
17 Y. Plyuto, J. M. Berquier, C. Jacquiod and C. Ricolleau, *Chem. Commun.*, 1999, 1653.
18 Y. Guari, C. Thieuleux, A. Medhi, C. Reye, R. J. P. Corriu, S. Gomez-Gallardo, K. Philippot, B. Chaudret and R. Dutartre, *Chem. Commun.*, 2001, 1374.
19 P. Mukherjee, C. R. Patra, R. Kumar and M. Sastry, *Phys. Chem. Commun.*, 2001, **5**, 1.
20 M. H. Huang, A. Choudrey and P. Yang, *Chem. Commun.*, 2000, 1063.
21 W. Chen, W. Cai, L. Zhang, G. Wang and L. Zhang, *J. Colloid Interface Sci.*, 2001, **238**, 291.
22 C. M. Yang, H. S. Sheu and K. J. Chao, *Adv. Funct. Mater.*, 2002, **12**, 143.
23 Ö. Dag, A. Verma, G. A. Ozin and C. T. Kresge, *J. Mater. Chem.*, 1999, **9**, 1475.
24 O. Samarskaya and Ö. Dag, *J. Colloid Interface Sci.*, 2001, **238**, 203.
25 Ö. Çelik and Ö. Dag, *Angew. Chem. Int. Ed.*, 2001, **40**, 3800.
26 Ö. Dag, I. Soten, Ö. Çelik, S. Polarz, N. Coombs and G. A. Ozin, *Adv. Funct. Mater.*, 2003, **13**, 30.
27 Y. S. Tang, S. J. Cai, G. L. Jin, K. L. Wang, H. M. Soyer and B. S. Dunn, *Thin Solid Films*, 1998, **321**, 76.
28 Y. Plyuto, J.-M. Berquier, C. Jacquiod and C. Ricolleau, *Chem. Commun.*, 1999, 1653.
29 S. Besson, T. Gacoin, C. Ricolleau, C. Jacquiod and J.-P. Boilot, *Nano Lett.*, 2002, **2**, 409.
30 H. Schott, *J. Colloid Interface Sci.*, 1997, **192**, 458.
31 M. E. Fragala, G. Malandiro and O. Puglisi, *Chem. Mater.*, 2000, **12**, 290.
32 W. Wiecrorek, D. Raducha, A. Zalewska and J. R. Stevens, *J. Phys. Chem. B*, 1998, **102**, 8725.
33 Y. Nibu and T. Inoue, *J. Colloid Interface Sci.*, 1998, **205**, 231.
34 V. D. Noto, D. Longo and V. Münchow, *J. Phys. Chem. B*, 1991, **101**, 2636.
35 H. Matsura, K. Fukuhara, K. Takashima and M. Sakokibara, *J. Phys. Chem.*, 1991, **95**, 10800.
36 N. Kimura, J. Umemura and S. Hayashi, *J. Colloid Interface Sci.*, 1996, **182**, 356.
37 Ö. Dag, O. Samarskaya, C. Tura, A. Günay and Ö. Çelik, *Langmuir*, submitted.
38 G. S. Attard, P. N. Bartlett, N. R. B. Coleman, J. M. Elliott and J. R. Owen, *Langmuir*, 1998, **14**, 7340.
39 D. H. Gray and D. L. Gin, *Chem. Mater.*, 1998, **10**, 1827.
40 Q. Huo, D. I. Margulese and G. D. Stucky, *Chem. Mater.*, 1996, **8**, 1147.
41 J. M. Kim, Y. Sakamoto, Y. K. Hwang, Y.-U. Kwon, O. Terasaki, S.-E. Park and G. D. Stucky, *J. Phys. Chem. B*, 2002, **106**, 2552.
42 W. Cai, H. Hofmeister, T. Rainer and W. Chen, *J. Nanoparticle Res.*, 2001, **3**, 443.